On the influence of the AC voltage on the dynamics of electrically actuated geometrically nonlinear clamped rectangular micro- and nanoplates

Andrianov, Igor V.; van Horssen, Wim T.; Koblik, Steve G.; Starushenko, Galina A.

DOI
10.1007/s11071-025-11307-9

Publication date
2025

Document Version
Final published version

Published in
Nonlinear Dynamics

Citation (APA)
Andrianov, I. V., van Horssen, W. T., Koblik, S. G., & Starushenko, G. A. (2025). On the influence of the AC voltage on the dynamics of electrically actuated geometrically nonlinear clamped rectangular micro- and nanoplates. *Nonlinear Dynamics*, *113*(17), 22489-22506. https://doi.org/10.1007/s11071-025-11307-9

Nonlinear Dyn
https://doi.org/10.1007/s11071-025-11307-9

RESEARCH

On the influence of the AC voltage on the dynamics of electrically actuated geometrically nonlinear clamped rectangular micro- and nanoplates

Igor V. Andrianov · Wim T. van Horssen · Steve G. Koblik · Galina A. Starushenko

Received: 12 December 2024 / Accepted: 25 April 2025

Abstract The vibrations of electrically actuated micro- and nano rectangular plates, described by strongly nonlinear PDEs, are considered. The geometric nonlinearity is taken into account within the Berger model. One of the essentially nonlinear effects is the pull-in phenomenon, i.e., the transition from the oscillatory regime to the attracting one. A simple and physically justified algorithm for determining the voltage for which the system collapses is proposed. The algorithm is based on the detection of the voltage that leads to the merging of stable (center) and unstable (saddle) equilibrium points. The model and algorithm were validated by comparing them with other existing results in the literature, which were obtained by using the Galerkin method and FEM. The closeness of these results confirmed the adequacy of the adopted model and the high accuracy of the algorithm used in this paper. The study was conducted for a wide range of frequency changes and amplitude ratios of DC and AC voltages. Along with the determination of the pull-in voltages, the change in displacements over time was also studied. A spectral analysis was performed, which allows us to analyze the relationships between the input frequencies and the response spectra. The presence of the AC can lead to a dramatic decrease of the pull-in values. This is caused by resonances. The resonances arising in the system have a dual character. This can be either a nonlinear resonance caused by force excitation or a parametric resonance. A separate study was conducted to determine the nature of the emerging resonances. This provides useful information in practical situations. Knowing the resonant frequencies allows us to avoid them in operating electromechanical systems. This can be done by changing the frequency of the alternating voltage or by changing the ratio of the parameters of the system itself. The amplitude of the nonlinear resonance caused by force excitation can be reduced by introducing linear or nonlinear damping. Knowledge of resonant frequencies allows us to design new more effective electromechanical systems.

I. V. Andrianov (✉)
Chair and Institute of General Mechanics, RWTH Aachen University, Eilfschornsteinstrasse 18, 52062 Aachen, Germany
e-mail: igor.andrianov@gmail.com

W. T. van Horssen
Faculty EEMCS, Delft Institute of Applied Mathematics, Delft University of Technology, Mekelweg 4, 2628 CD Delft, The Netherlands
e-mail: W.T.vanHorssen@tudelft.nl

S. G. Koblik
Independent Researcher, 8110 Birchfield Drive, Indianapolis, IN 46268, USA
e-mail: stevekoblik8110@comcast.net

G. A. Starushenko
Dnipro University of Technology, Av. Dmytra Yavornytskoho, 19, Dnipro 49005, Ukraine
e-mail: gs.gala.star@gmail.com

Published online: 29 May 2025

Keywords MEMS · NEMS · AC voltage · DC voltage · Nonlinearity · Vibration · Dynamic pull-in

1 Introduction

MEMS and NEMS are now widespread and can be found in, for instance, actuators, switches, micro-mirrors, pressure sensors, moving valves, micro-grippers, electronics on a common silicon substrate, etc. [1–5]. They combine such useful properties as small size, light weight, inexpensive operation, and low-power consumption. MEMS and NEMS are usually used at the device level to reduce needed power, data transmission, and processing. Microfabrication technology is widely used. Let us give just a few examples. Capacitive MEMS-based ultrasonic transducers are used for the generation and detection of ultrasound waves in air and water [6, 7]. Chains of MEMS may be turned into transmission lines and support propagation of solitary waves [8]. A smart resonant gas sensor being capable of quantifying the amount of absorbed gas, can be autonomously triggered as an electrical switch upon exceeding a preset threshold of absorbed gas [9]. This list can be significantly expanded. One can find a comprehensive overview and background on work on micro- and nanostructures in [10, 11].

MEMS and NEMS are interesting and attractive systems offering unique and smart technological solutions. In this regard, accurate modeling the mechanical behavior of such structures is important. However, the following difficulties might arise. The electric forces are inherently strongly nonlinear. The micro- and nanoscale components undergo large deflections, that is why geometric nonlinearity is significant. Therefore, the mathematical models for MEMS and NEMS contain power and non-power nonlinearities and are difficult to analyze.

To solve the corresponding boundary value problems, both numerical and analytical methods are used. Of the numerical methods, the most widely used ones are the finite element method (FEM) [12–14] and the finite difference method (FDM) [15, 16]. These methods are computationally expensive. So, the development of efficient and accurate analytical methods is necessary to describe the behavior of the MEMS and NEMS.

Analytical approximations are usually constructed with methods from the field of Nonlinear Dynamics [11]. Even if not completely analytical approximations of solution are obtained, they allow one to simplify the problem in such a way that the desired answer is obtained with an extremely limited computational effort.

The most common MEMS and NEMS models are continuous systems such as beam, arches, plate and panel models [1–4, 17], described by PDEs. In the analysis these PDEs are replaced by systems of nonautonomous ODEs using the Galerkin (Kantorovich) method or another variational method. The resulting infinite systems of ODEs in time are truncated with varying degrees of justification. Reduced Order Model (ROM) is often used for this purpose [12, 14, 18–20]. Analysis in which cases truncation is allowed for an actuated beam problem is performed in [21].

In addition to discretization of continuous systems, it is possible to construct phenomenological models with a finite number of degrees of freedom [22–25]. They are formulated as ODE problems which include linear and nonlinear terms with unknown parameters. Based upon experiments, one fits the unknown parameter with different kind of methods to the obtained measurements, such that the experiments and the model equations give more or less the same bifurcations and amplitude-frequency responses. The disadvantage of these models is their low accuracy and the difficulty of refining the results obtained from these restricted measurements and experiments.

A multiple time-scales perturbation approach in order to obtain approximations of the solutions of the initial-boundary value problem allows one to describe well the behavior of an electromechanical system for small DC and AC voltages [21]. When studying near threshold (pull-in) values of DC and AC voltages, this method also allows one to obtain useful qualitative information [26]. The averaging theory [23] was also used for this purpose.

The problems under consideration are essentially nonlinear, and one of the essentially nonlinear effects is the pull-in phenomenon, i.e., the transition from the oscillatory regime to the attracting one. Dynamic pull-in in microelectromechanical systems is a special case of the problem of escape from a potential well under the influence of external forcing [7] or parametric excitation [27]. In [7] the authors studied the minimal

amplitude of external forcing needed for the pull-in (escape). The simplest one degree of freedom model with a linear spring is used. Authors suggested several fourth order polynomials to approximate the original electrostatic potential. The quality of predicting the escape threshold is assessed numerically. As a result, it is possible to obtain an approximate analytical description of the system's behavior in the vicinity of the primary resonance.

The most studied continuous models of MEMS and NEMS are beams and circular plates [1–4, 21]. Rectangular plates were less studied [12–16, 18–20, 26, 28–30]. What these papers have in common is the use of Kirchhoff's plate theory [12, 14, 15, 18–20, 26, 28] and von Kármán's nonlinear strain–displacement relations [12–14, 18, 19, 26, 28]. Sometimes also Berger's model is used [15, 20]. Of the numerical methods used, FEM and FDM can be mentioned [12, 13, 15, 16, 20]. Analytical and numerical-analytical solutions are based on the Kantorovich (Galerkin) method [12–15, 18–20, 26, 29, 30], often in combination with ROM [12, 14, 18, 19]. As a rule, the plates are considered to be clamped at the edges [12–14, 18–20, 26, 28, 29]. The aforementioned papers study the influence of various factors on the pull-in voltage and the pull-in deflection for rectangular electrically actuated micro- and nanoplates. The combined effects of van der Waals force and thermal stresses were analysed in [19], and the influence of the Casimir force was estimated in [18]. The relationship between lumped and continuous models is analyzed in [20]. The theoretical results are validated by FEM and experimental studies. In [28] the couple stress theory is employed to model the small-size effects. The in-plane and out-of-plane motions were analysed. The Floquet theory is used in the stability analysis. The effect of different boundary conditions was studied in [26], and the multiple time-scales perturbation method was used to describe the transient behavior of the system. Analytical results were validated by numerical simulations. Actuated rectangular microplates on a movable base with in plane loading where considered in [29]. The results show that for a movable base the MEMS pull-in voltage is much lower than for a fixed substrate. The tension in-plane loading increases the pull-in value, whereas midplane compression decreases this value. In [15] the dynamic pull-in for an electrostatically actuated microplate is analyzed based on Berger's plate theory. The obtained results were compared with experimental studies and good agreement was achieved. This validated the applicability of Berger's model to the study of an electrically actuated rectangular microplate. In [30] the use of a piezoelectric layers to reduce the sound radiation transmitted through and radiated by an aluminum plate immersed in a light fluid was studied. As a model, the authors considered an infinite plate with piezoelectric layers separating two half spaces filled with two identical light fluids. They analysed how a sound wave is transmitted through the plate. In [12] the forced vibration response of the plate is then investigated when the plate is excited by a harmonic AC load superimposed to a DC load. The dynamic behavior is examined near the primary and secondary (superharmonic and subharmonic) resonances. The microplate shows a strong hardening behavior due to the cubic geometrical nonlinearity. However, the behavior switches to softening as the DC load is increased. Finally, near-square plates are studied to understand the effect of geometric imperfections of microplates. The electrostatically actuated microstructures subjected to nonlinear squeezed film damping and in-plane forces are investigated in [16]. First-order shear deformation theory is used to model the dynamical system by means of FEM. The nonlinear Reynolds equation for the squeezed film damping are solved by FDM. The influence of the squeezed-film damping on the dynamic behavior and on the pull-in values for electrically actuated rectangular micro plates is also studied in [13].

In [31, 32] an effective algorithm was proposed to analyze the pull-in phenomenon for thin-walled MEMS/NEMS. As a result the following conclusions were made:

1. The influence of a geometric nonlinearity on the behaviour of MEMS/NEMS is significant and cannot be neglected.
2. The impact of the van der Waals force is more significant than that of the Casimir force and significantly less than the influence of the Coulomb force.
3. If the energy of the system is small (that is, the system is far from pull-in), then an approximation of the original nonlinearity by a low-order polynomial (up to order 6) is justified. When the energy of the system is near the pull-in value, then

only high-order polynomial approximations (that is, polynomials of degree 15 or higher) give satisfactory results.

The aforementioned conclusions were made in [31, 32] based on the study of lumped systems, beams, and circular micro- and nanoplates. Only the static pull-in phenomena were investigated in [31, 32]. On the other hand, the algorithm developed in [31, 32] allows us to solve more complex problems. By using the algorithm in this paper, we study dynamic pull-in phenomena, its features, and the relationships between static and dynamic pull-in values. A rectangular plate was chosen as the object of study. The reason for this choice is that such an object successfully describes many typical devices [1–5]. The availability of papers with simulations of such devices [12, 15] allows us to test the algorithm, and to show its accuracy. Based on the results of [31, 32], we take into account geometric nonlinearity of the rectangular plate, and limit ourselves to the Coulomb force (without using polynomial approximations of this force).

This paper is organized as follows. The original boundary value problem is described in Sect. 2. It consists of a PDE and some boundary and initial conditions. Then, the original boundary value problem is rewritten in a dimensionless form. In Sect. 3 the boundary value problem for the PDE is reduced to an initial value problem for an ODE by using the Kantorovich method. Section 4 is devoted to the study of the asymptotic behavior of the integrals which occur in the obtained ODE. A numerical algorithm is described in Sect. 5 to solve a static pull-in problem. Validation of the algorithm is described in Sect. 6. Pull-in values and critical displacements were compared with Galerkin and FEM studies by other authors and good agreement was achieved. The obtained phase portraits and frequencies are analysed in Sect. 7. Properties of dynamical pull-in are described in Sect. 8. A spectral analysis of the obtained results is carried out in Sect. 9. Section 10 is devoted to the analysis of resonances arising under the influence of an AC voltage. Finally, in Sect. 11 some concluding remarks are presented.

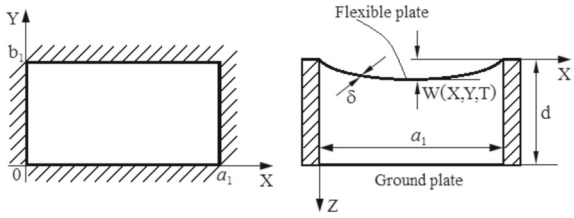

Fig. 1 Top and cross-section views of a model of the parallel charged micro/nano rectangular plates. Displacement towards the ground plate is considered to be positive, and movement in the opposite direction is considered to be negative

2 Governing equations

The equation to describe the nonlinear vibrations of a rectangular nanoplate (see Fig. 1) under the action of Coulomb, Casimir and van der Waals forces can be written as follows

$$\rho\delta\frac{\partial^2 W}{\partial T^2}+\Gamma\frac{\partial W}{\partial T}+D\left(\frac{\partial^2}{\partial X^2}+\frac{\partial^2}{\partial Y^2}\right)^2 W - \frac{B}{2a_1b_1}\left(\int_0^{a_1}\int_0^{b_1}\left(\left(\frac{\partial W}{\partial X}\right)^2+\left(\frac{\partial W}{\partial Y}\right)^2\right)dXdY\right) - \frac{\varepsilon^*\varepsilon_0\left(V_0+V_1\sin\Omega T\right)^2}{2(d-W)^2}-\frac{H}{6\pi(d-W)^3} - \frac{\overline{h}c\pi^2}{240(d-W)^4}=0, \tag{1}$$

where ρ is the plate mass density, δ is the plate thickness, Γ is the linear damping coefficient, $B=\frac{E\delta}{1-\nu^2}$ is the membrane rigidity, $D=\frac{E\delta^3}{12(1-\nu^2)}$ is the flexural rigidity, ν is the Poisson coefficient, E is the Young modulus, ε^* is the relative permittivity of the medium between the ground plate and the flexible plate, ε_0 is the vacuum permittivity ($\varepsilon_0=8.85\cdot10^{-12}$ F/m), V_0, V_1 are the magnitudes of the DC and the AC voltage, Ω is the AC frequency, H is the Hamaker constant, $\overline{h}$ is the reduced Plank constant, c is the speed of light in vacuum, d is the gap between the flexible MEM/NEMS rectangular plate and the ground plate (see Fig. 1), T is the time, X, Y are the spatial variables with $0\le X\le a_1, 0\le Y\le b_1$(where a_1 and b_1 are the width and length of the flexible plate, respectively (see Fig. 1)), and $W(X,Y,T)$ is the normal displacement,

positive towards the ground plate (see Fig. 1), that is, in the Z-direction (see Fig. 1).

The last two terms in Eq. (1) describe the van der Waals and the Casimir forces. These forces describe the same phenomenon but at different scales and cannot be taken into account simultaneously. The distributed load due to the Casimir force per unit surface area is given by the proximity force approximation [19, 33]. For gaps smaller than the retardation length, that is, for gaps smaller than the wavelength of the virtual transitions responsible for the quantum dipole fluctuations [34], the Casimir force reduces to the van der Waals distributed force [35].

It is assumed that the plate is clamped along the contour, so that the displacements of the plate in the plane on the contour is zero. This makes it possible to use Berger's hypothesis [36] and sufficiently simplifies the original nonlinear boundary value problem, reducing them to one PDE (1).

Berger's equation was used previously in the study of circular electrically actuated plates [32]. A comparison between the results based on the von Kármán and Berger models showed their closeness. This conclusion is also confirmed by the results obtained in [37–39], devoted to other problems.

The boundary conditions for the normal displacement $W(X, Y, T)$ are:

$$\begin{aligned} &W = 0 \ \text{ at } X = 0,\ a_1,\ Y = 0,\ b_1; \\ &\frac{\partial W}{\partial X} = 0 \text{ at } X = 0,\ a_1,\ \frac{\partial W}{\partial Y} = 0 \text{ at } Y = 0,\ b_1; \end{aligned} \tag{2}$$

We assume to have zero initial conditions:

$$W|_{T=0} = 0,\ \left.\frac{\partial W}{\partial T}\right|_{T=0} = 0 \tag{3}$$

Let us introduce the dimensionless variables:

$$\begin{aligned} &x = X/a_1;\ y = Y/b_1; \quad b = b_1/a_1; \\ &t = \frac{T}{a_1^2}\sqrt{\frac{D}{\rho\delta}};\ \ w(x,\ y,\ t) = W(X, Y, T)/d. \end{aligned} \tag{4}$$

In dimensionless variables Eq. (1) takes the form

$$\begin{aligned} &\frac{\partial^2 w}{\partial t^2} + \xi\frac{\partial w}{\partial t} + \left(\frac{\partial^4 w}{\partial x^4} + \frac{2}{b^2}\frac{\partial^4 w}{\partial x^2\partial y^2} + \frac{1}{b^4}\frac{\partial^4 w}{\partial y^4}\right) \\ &- B_1\left(\int_0^1\int_0^1\left(\left(\frac{\partial w}{\partial x}\right)^2 + \frac{1}{b^2}\left(\frac{\partial w}{\partial y}\right)^2\right)dxdy\right) \\ &\left(\frac{\partial^2 w}{\partial x^2} + \frac{1}{b^2}\frac{\partial^2 w}{\partial y^2}\right) - \frac{(\alpha + \alpha_1\sin\omega t)^2}{(1-w)^2} - \frac{\beta}{(1-w)^3} \\ &- \frac{\gamma}{(1-w)^4} = 0, \end{aligned} \tag{5}$$

$$\begin{aligned} &\text{where } B_1 = \frac{d^2}{2D}B, \xi = \frac{a_1^2}{\sqrt{\rho\delta D}}\Gamma, \alpha = \frac{a_1^2 V_0}{d}\sqrt{\frac{\varepsilon^*\varepsilon_0}{2dD}}, \\ &\alpha_1 = \frac{a_1^2 V_1}{d}\sqrt{\frac{\varepsilon^*\varepsilon_0}{2dD}}, \omega = a_1^2\Omega\sqrt{\frac{\rho\delta}{D}}, \beta = \frac{a_1^4 H}{6\pi d^4 D}, \\ &\gamma = \frac{a_1^4\overline{h}c\pi^2}{240d^5 D}. \end{aligned} \tag{6}$$

The boundary and initial conditions in dimensionless variables are:

$$\begin{aligned} &w = 0 \text{ at } x = 0, 1;\ y = 0, 1;\ \frac{\partial w}{\partial x} = 0 \text{ at } x = 0, 1; \\ &\frac{\partial w}{\partial y} = 0 \text{ at } y = 0, 1, \end{aligned} \tag{7}$$

$$w|_{t=0} = 0,\ \left.\frac{\partial w}{\partial t}\right|_{t=0} = 0. \tag{8}$$

3 Reducing the original PDE to an ODE

For reducing the original PDE (5) to an ODE we use the following ansatz, which satisfies the boundary conditions (7):

$$w(x,\ y,\ t) \approx u(t)\sin^2(\pi x)\sin^2(\pi y) \tag{9}$$

Ansatz (9) gives a good approximation of the solution of the original problem. For the first natural frequency of a linear square plate, using approximation (9), one obtains $\omega_1 \approx 37.22$. The value, obtained by a numerical procedure [40], is $\omega_1 \approx 35.988$.

Now we use the Kantorovich procedure [41]. According to this method, we substitute expression (9) into Eq. (5), multiply the so-obtained expression by $\sin^2(\pi x)\sin^2(\pi y)$, and integrate with respect to x

and y over the domain $0<x<1$ and $0<y<1$. As a result, one obtains:

$$\ddot{u}+\xi\dot{u}+c_1u+c_3u^3+(\alpha+\alpha_1\sin\omega t)^2I_1(u)+\beta I_2(u)+\gamma I_3(u)=0, \tag{10}$$

where $\dot{u}=\frac{du}{dt}$, $c_1=\frac{16\pi^4}{9}\left(3+\frac{2}{b^2}+\frac{3}{b^4}\right)$, $c_3=\frac{\pi^4}{4}B_1\left(1+\frac{1}{b^2}\right)^2$, $I_k(u)=\int_0^1\int_0^1\frac{\sin^2(\pi x)\sin^2(\pi y)}{\left(1-u\sin^2(\pi x)\sin^2(\pi y)\right)^{k+1}}\,dxdy$, $k=1,2,3$.

Since the influence of damping is small, we first examine the behavior of system (10) at $\xi=0$. In this case the potential energy of this system is given by

$$F=-\frac{d\Pi(u)}{du}=-\left[c_1u+c_3u^3+(\alpha+\alpha_1\sin\omega t)^2I_1(u)+\beta I_2(u)+\gamma I_3(u)\right] \tag{12}$$

In the absence of parametric excitation (that is, $\alpha_1=0$) Eq. (10) turns out to be autonomous and studying the derivative of the potential energy allows us to obtain a complete qualitative picture of the mass movement.

The integrals $I_k(u)$ are expressed through the complete elliptic integrals of the first and the second kind

$$I_1(u)=\begin{cases}-\dfrac{64(1-k^2)^{3/2}}{9\pi k^2}(K(k)-E(k)), & u\le 0,\quad 0\le k=\sqrt{\dfrac{-u}{1-u}}<1,\\ \dfrac{64}{9\pi u}\left(K\left(\sqrt{u}\right)-\dfrac{1}{1-u}\mathrm{E}\left(\sqrt{u}\right)\right), & 0\le u<1,\end{cases}$$

$$I_2(u)=\begin{cases}-\dfrac{16(1-k^2)^{3/2}}{9\pi k^2}\left(\left(2-k^2\right)K(k)-2E(k)\right), & u\le 0,\quad 0\le k=\sqrt{\dfrac{-u}{1-u}}<1,\\ \dfrac{16}{9\pi u(1-u)}\left((2-u)K\left(\sqrt{u}\right)-\dfrac{2}{1-u}E\left(\sqrt{u}\right)\right), & 0\le u<1,\end{cases}$$

$$I_3(u)=\begin{cases}\dfrac{8}{27\pi u(1-u)^{5/2}}\left(\left(8-7u+3u^2\right)\mathrm{K}(k)-\left(8+u-u^2\right)\mathrm{E}(k)\right), & u\le 0,\quad 0\le k=\sqrt{\dfrac{-u}{1-u}}<1,\\ \dfrac{8}{27\pi u(1-u)^2}\left(\left(8-7u+3u^2\right)K\left(\sqrt{u}\right)-\dfrac{8+u-u^2}{1-u}E\left(\sqrt{u}\right)\right), & 0\le u<1.\end{cases} \tag{13}$$

$$\Pi(u)=c_1\frac{u^2}{2}+c_3\frac{u^4}{4}+\int_0^u\left[(\alpha+\alpha_1\sin\omega t)^2I_1(u)+\beta I_2(u)+\gamma I_3(u)\right]du \tag{11}$$

Equation (10) describes the motion of a point mass under the action of a force F that depends on the displacement u and time t, where:

4 The asymptotic behavior of the integrals $I_k(u)$

We will use properties of the complete elliptic integrals [42] to describe the behavior of $I_k(u)$ for k = 1,2,3. The functions $I_k(u)$ are continuous on the open interval $(-\infty,\ 1)$. For $u\to-\infty$ these functions tend to zero as $O\left(|u|^{-3/2}\ln(|u|)\right)$. Their behavior for $u\to-\infty$ is as follows:

$$
\begin{aligned}
I_1(u) &= \frac{64\ln 4\sqrt{1-u}}{9\pi u\sqrt{1-u}} + O\left(|u|^{-3/2}\right),\\
I_2(u) &= \frac{16\ln 4\sqrt{1-u}}{9\pi u\sqrt{1-u}} + O\left(|u|^{-3/2}\right),\\
I_3(u) &= \frac{8\ln 4\sqrt{1-u}}{3\pi u\sqrt{1-u}} + O\left(|u|^{-3/2}\right)
\end{aligned}
\tag{14}
$$

At $u = 0$ one obtains $I_1(u) = I_2(u) = I_3(u) = -16/9$, and for $u \to 1$ the functions $I_k(u)$ tend to $-\infty$ in the following way:

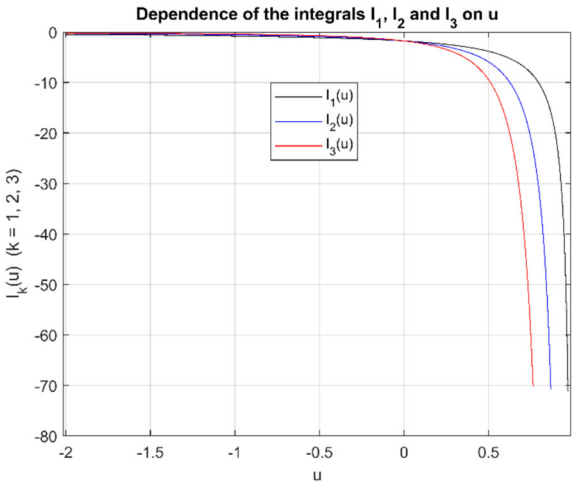

Fig. 2 Behavior of the integrals $I_k(u)$, $k = 1, 2, 3$ in the interval $(-2, 1)$

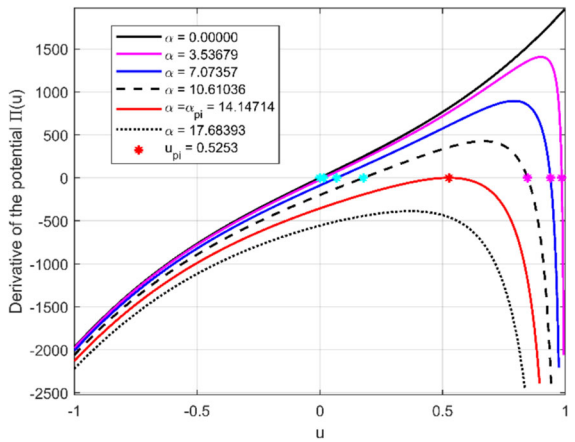

Fig. 3 Dependence of the derivative of the potential energy on the displacement u

$$
\begin{aligned}
I_1(u) &\approx -\frac{1}{\pi(1-u)} + O(\ln(1-u)),\\
I_2(u) &\approx -\frac{1}{2\pi u(1-u)^2} + O\left(\frac{1}{(1-u)}\right),\\
I_3(u) &\approx -\frac{1}{3\pi u(1-u)^3} + O\left(\frac{\ln(1-u)}{(1-u)^2}\right).
\end{aligned}
\tag{15}
$$

The behavior of the functions $I_k(u)$, $k = 1, 2, 3$, is shown in Fig. 2. This behavior is quite consistent with the physics of the phenomenon, namely:

1) For $u \to -\infty$ the moving plate of the capacitor is on average of a large distance from the ground plate, which leads to an almost zero interaction force between the plates.
2) For $u \to 1$ the distance between the capacitor plates decreases to zero, which leads to an extremely large interaction force between the plates.
3) When $u = 1$ for certain x and y values the moving and ground plates touch each other. This means that investigating the plate system does not make sense from the physical standpoint.

The dependence of the derivative of the potential energy of the point mass on the displacement u in the absence of parametric excitation ($\alpha_1 = 0$) can be described as follows

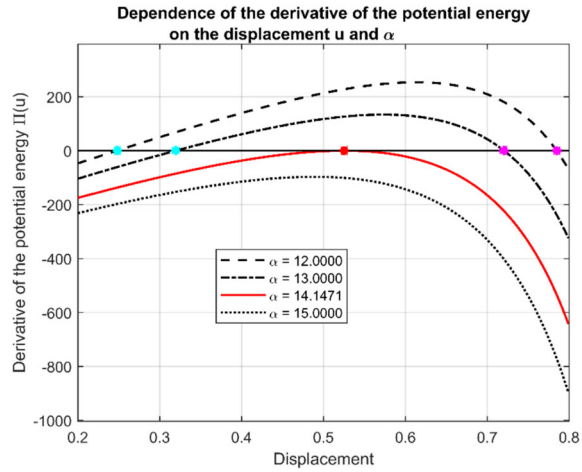

Fig. 4 Dependence of the derivative of the potential energy $\Pi(u)$ on the displacement for various values of the parameter α. The other parameters are defined in (17)

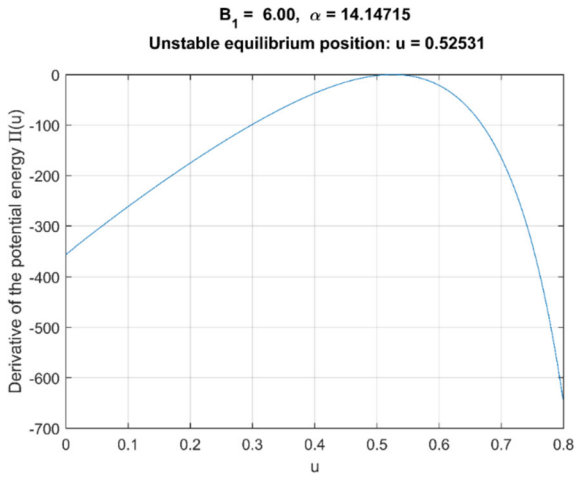

Fig. 5 Dependence of the derivative of the potential energy $\Pi(u)$ on the displacement u when parameter α reaches a pull-in value. The other parameters are defined in (17)

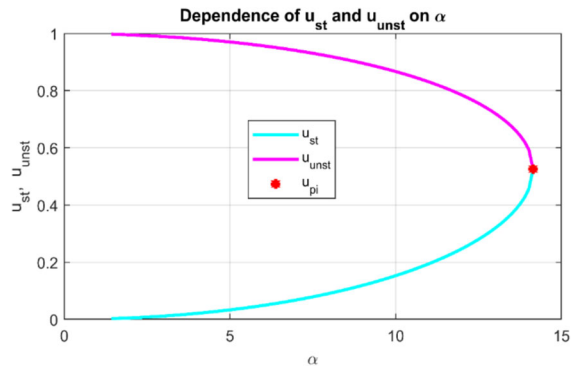

Fig. 6 Positions of the equilibrium points for various values of the parameter α. The other parameters are defined in (17). Red point correspondences to a saddle-node bifurcation point

$$\frac{d\Pi}{du} = \psi = \psi_1 + \psi_2, \qquad \psi_1 = c_1 u + c_3 u^3, \\ \psi_2 = \alpha^2 I_1(u) + \beta I_2(u) + \gamma I_3(u) \tag{16}$$

In Fig. 3 function ψ for different values of the parameter α is given. The other parameter values were chosen as in [12]:

$$b = 1, B_1 = 6.00, \alpha_1 = \beta = \gamma = 0 \tag{17}$$

These parameter values correspond to real MEMS.

Since I_k, $k = 1, 2, 3$ tend to zero for $u \to -\infty$, it can be expected that for $u < -1$ the values of the function ψ tend to the values of the function ψ_1 (see Eq. (15) and Fig. 3). As α is non-negative, the derivative of the potential energy (11) is less than zero at the point $u = 0$.

For the given parameters in (17) one obtains $c_1 = 1385.4$ and $c_3 = 584.5$. When the parameter α changes in the interval $0 \le \alpha \le 12$, and since the coefficients c_1 and c_3 are two orders of magnitude larger than α, then for small values of u the value of ψ is positive (that is, the function ψ_1 is dominant). When the value of u approaches 1, the function ψ_2 becomes dominant and the expression for ψ becomes negative. Thus, the derivative of the potential energy can change sign at least twice.

5 Algorithm for calculating the pull-in values

Let us describe the algorithm to calculate the pull-in, assuming for simplicity and without loss of generality that $\alpha_1 = 0$. Figure 4 shows the dependence of the derivative of the potential energy on the displacement u for various values of the parameter α and the parameters as given in (17). Stationary values correspond to the points of intersection of the graph with the line $\psi = 0$. The points marked by a cyan colour

Table 1 Comparison of the pull-in values obtained in this paper and those obtained in [12] by a Galerkin approach and FEM

b/a	α_{pi}[12]	α_{pi} this paper	Diff. %
1.0	192	200	+ 4.2
1.1	160	166	+ 3.8
1.2	139	143	+ 2.9
1.5	107	108	+ 0.9
2.0	88	87	− 1.1
20.0	73	64	− 12.3

Table 2 Comparison of the pull-in displacements obtained in this paper and those obtained in [12] by a Galerkin approach and FEM

b/a	u_{pi}[12]	u_{pi} this paper	Diff. %
1.0	0.50	0.525	+ 5.0
1.1	0.50	0.520	+ 4.0
1.2	0.50	0.527	+ 5.4
1.5	0.49	0.507	+ 3.5
2.0	0.49	0.498	+ 1.6
20.0	0.48	0.479	− 0.2

determine the stable equilibrium positions (that is, center points), and the points marked by a magenta colour describe the unstable ones (that is, saddle points). As α increases, the distance between the stable and unstable points decreases. As is shown in [31, 32], using the theory of stability for ODEs [43], if neighboring points of stable and unstable equilibrium merge, the result is a point of an unstable equilibrium. Indeed, since the derivative of the potential energy vanishes at the adjacent equilibrium points, there must be an extreme point of the derivative of the potential energy between them, at which the second derivative of the latter is equal to zero. Therefore, at the point of confluence, both the first order and the second order derivatives of the potential energy are equal to zero. So, the coincidence of the points defines a pull-in value α_{pi} and a pull-in displacement u_{pi}(red points in Fig. 4).

So, if at some value of the parameter α the stable and unstable points coincide, the local maximum of the curve moves down to the line on which the derivative of potential energy is equal to zero. This line becomes tangent to the graph (see Fig. 5). The algorithm tracks the change in the position of this maximum following the parameter changes and fixes its hit on the line $\frac{d\Pi(u)}{du} = 0$. The merging of the stable and unstable equilibrium points is also shown in Fig. 6 as a red dot.

6 Validation of the algorithm

To estimate the accuracy of the algorithm, we use the results from the paper [12]. We suppose $B_1 = 6.00, \alpha_1 = \beta = \gamma = 0$. Comparing of our results with corresponding results from the paper [12] for plates with various aspect ratios shows a good agreement (see Tables 1 and 2).

In [12] a geometric nonlinearity was taken into account within the framework of the von Kármán model, whereas we are using the Berger equation. Also in [12] a ROM approach was used, and we applied the Kantorovich procedure. Despite these differences, the values for the pull-in voltage and maximum displacements are close to each other. Let us also note that in [12] an excellent agreement was found for the results calculated by the ROM approach and a FEM approach. Thus, three significantly different approaches give similar results.

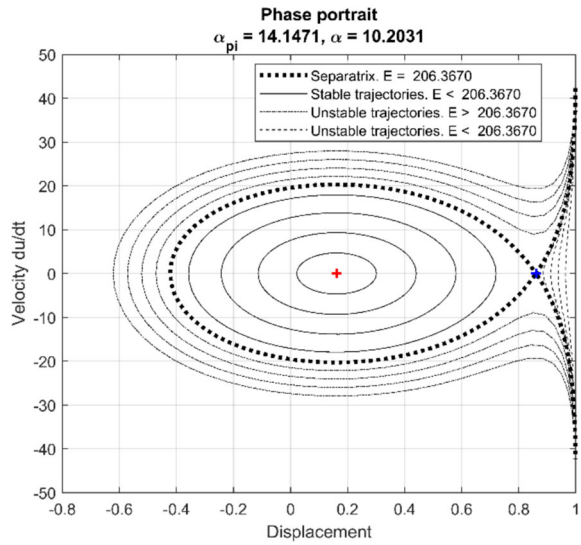

Fig. 7 The phase portrait of the system for various energies, and for parameter values as given in (17)

7 Phase portrait and vibration frequencies for a constant applied voltage

Let us denote by u_{gpd} the point of greatest positive displacement of the system. If one deflects the movable plate relative to the stable equilibrium position u_{st} at a constant voltage α to the position $u_{gpd} < u_{unst}$ and releases it, then the system will oscillate relative to the point u_{st}. The potential energy of these elastic vibrations is determined by the formula

$$\Pi_{st}(u) = \Pi(u) - \Pi(u_{st}) = c_1 \frac{u^2 - u_{st}^2}{2} + c_3 \frac{u^4 - u_{st}^4}{4} + \int_{u_{st}}^{u} \left[\alpha^2 I_1(u) + \beta I_2(u) + \gamma I_3(u)\right] du, \qquad u \le u_{gpd} \tag{18}$$

The total energy of motion of a conservative autonomous system is constant, and equal to

$$E = \frac{\dot{u}^2}{2} + \Pi_{st}(u) \equiv const \tag{19}$$

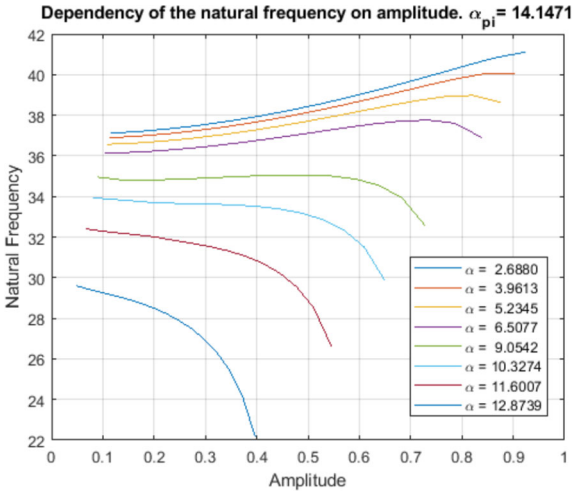

Fig. 8 Dependency of the natural frequencies on the amplitudes. The calculations were carried out for parameter values as given in (17)

We use Eq. (19) to determine the point of greatest negative deviation of the system given by u_{gnd}, that is, we use

$$E - \Pi_{st}(u_{gnd}) = 0 \tag{20}$$

This allows us to obtain a phase portrait of the system, described by the formula.

$$\frac{du}{dt} = \pm\sqrt{2(E - \Pi_{st}(u))} \tag{21}$$

The phase portrait of the system for $\alpha < \alpha_{pi}$ is shown in Fig. 7. The thick black dots represent the separatrix, which separates the areas of stable and unstable motions. The solid thin lines indicate the area of stable (periodic) motions. The calculations were carried out for the parameter values as given in (17).

The behavior of the solution near the line $u = 1$ is singular and has been described in Sect. 4. Periodic solutions of Eq. (10) are limited to the closed domain defined by the separatrix, and are only possible when $\alpha < \alpha_{pi}$. Maximum positive displacements during such periodic motions are restricted by the value $u_{\max} < u_{unst}$, and the corresponding energy is:

$$\Pi_{st}(u) = c_1 \frac{u_{\max}^2 - u_{st}^2}{2} + c_3 \frac{u_{\max}^4 - u_{st}^4}{4} + \int_{u_{st}}^{u_{\max}} \left[\alpha^2 I_1(u) + \beta I_2(u) + \gamma I_3(u)\right] du \tag{22}$$

The remaining part of the physically admitted domain of the phase plane consists of unstable (non-periodic) trajectories.

The periods of the natural vibrations T_{nf} and the natural frequencies ω_{nf} for given α and u_{gpd} are given by

$$T_{nf} = \sqrt{2} \int_{u_{gnd}}^{u_{gpd}} \frac{du}{\sqrt{E - \Pi_{st}(u)}} \text{ and } \omega_{nf} = \frac{2\pi}{T_{nf}} \tag{23}$$

respectively. Note that we deal with the first mode of vibration for the original system. In Fig. 8 the dependence of the frequency of the natural vibrations of the system on their amplitude are given for various values of α. The interval for the amplitudes decreases as α approaches α_{pi}, since the distance between u_{st} and u_{unst} decreases.

Figure 8 shows that at a low constant voltage, the natural frequency of the system first increases with increasing oscillation amplitude (due to the influence of a geometric nonlinearity), and then, as the amplitude approaches the unstable stationary point, the frequency decreases (due to the influence of the nonlinearity in the electrostatic forces). For a significantly large applied voltage, the natural frequency decreases with increasing amplitudes, since in this case the distance between the stable and the unstable stationary point is small, and the influence of electrostatic forces prevails throughout the entire amplitude range. Thus, when the parameter is increased, there is a change in behavior from hard nonlinear vibrations to the soft nonlinear vibrations. The indicated change is characteristic for the systems under consideration [1, 12].

8 Dynamic pull-in

In this Section we study the pull-in instability due to an applied DC and AC voltages. As is shown in [12, 44–46], this case strongly differs from those under a purely DC voltage. In particular, the use of an AC voltage can lead to a decrease in the DC pull-in voltage. This may be due to dynamic instabilities of various natures [46]. Such phenomenon is called dynamic pull-in.

Let us study the influence of the AC voltage on α_{pi}. To do this, we fix both the value of the DC voltage in

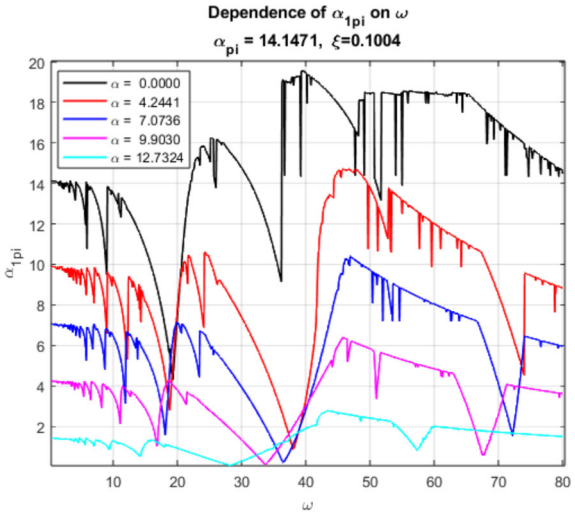

Fig. 9 Dependence of the pull-in value $\alpha_{1\,\mathrm{pi}}$ on the dimensionless frequency ω for various values of the DC voltage α. All other parameters are defined in (17)

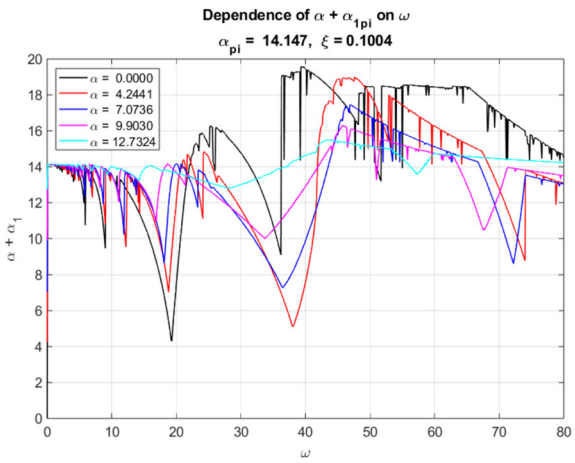

Fig. 10 Dependence of the pull-in value $\alpha_{1\,\mathrm{pi}}$ on the dimensionless frequency ω for different values of the sum of the amplitudes of the DC and AC voltages $\alpha + \alpha_{1\mathrm{pi}}$. The other parameters are defined in (17)

the interval $0 \le \alpha < \alpha_{pi}$, and the value of the dimensionless AC frequency ω. Then, we determine the values of u_{st} and u_{unst} corresponding to the fixed value of α. We take a certain value for the parametric excitation amplitude α_1. Equation (10) is then solved numerically (by the Runge–Kutta method) for the initial values

$$u(0) = u_{st}, \quad \dot{u}(0) = 0$$

over a large time interval (in this case, 80 units for t). In this case, using a binary search method, a value for $\alpha_{1\mathrm{pi}}$, was selected such that the solution to Eq. (10) does not exceed u_{unst} at $\alpha_1 = \alpha_{1\,\mathrm{pi}}$ and exceeds u_{unst} at $\alpha_1 = \alpha_{1\,\mathrm{pi}} + \varepsilon$, where $\varepsilon = 10^{-4}$. To check the reliability of this approach, the calculations were repeated using the following criterion: find a value $\alpha_{1\mathrm{pi}}$, such that the solution Eq. (10) is less than unity for $\alpha_1 = \alpha_{1\,\mathrm{pi}}$, and equal to or greater than one for $\alpha_1 \ge \alpha_{1\,\mathrm{pi}}$.The results of both calculations differ by less than 10^{-4}, which confirms the correctness of the chosen approach.

By varying ω, we obtain the dependence of $\alpha_{1\,\mathrm{pi}}$ on ω and α. Computations were carried out from $\omega = 0$ to a value $\omega = 80$, which is approximately twice the value of the natural frequency of the system. The step size was chosen to be 0.1. For convenience, the discrete points are connected by continuous curves, and these curves are given in Figs. 9 and 10. Periodic (stable) solutions of Eq. (10) correspond to points α_1 located below the graph $\alpha_{1\mathrm{pi}}(\alpha,\ \omega)$, and non-periodic (unstable) solutions correspond to points α_1 allocated above the specified graph.

It is interesting to compare intervals with different behavior of the curves with the value of the primary resonant frequency ω_{rf} of the original plate. As would be expected, at frequencies $\omega \le \omega_{rf}$ the amplitude of the AC voltage $\alpha_{1\,\mathrm{pi}}$ decreases with increasing DC voltage α. For low $(\omega \le \omega_{rf}/10)$ frequencies $\alpha + \alpha_{1\mathrm{pi}} \approx \alpha_{\mathrm{pi}}$, which corresponds to the results obtained in [12, 44–46].

In both Figs. 9 and 10, the curves separate the areas of periodic and non-periodic (unstable) modes. Below each curve there is an area of bounded and possibly periodic modes. The constructed dependencies are very irregular.

A significant decrease in both $\alpha_{1\mathrm{pi}}$ and $\alpha + \alpha_{1\mathrm{pi}}$ is observed at frequencies ω close to the primary resonance frequency ω_{rf} of the system. At frequencies ω close to $\omega_{rf}/5, \omega_{rf}/4, \omega_{rf}/3, \omega_{rf}/2$ superharmonic resonances are encountered and for frequencies ω close to $2\omega_{rf}$ subharmonic resonance is observed.

These results are qualitatively consistent with those obtained in [47] for beams and in [12] for rectangular plates. At the same time, the AC voltage can lead to a significant increase or decrease of the α_{pi} value in specific frequency ω intervals.

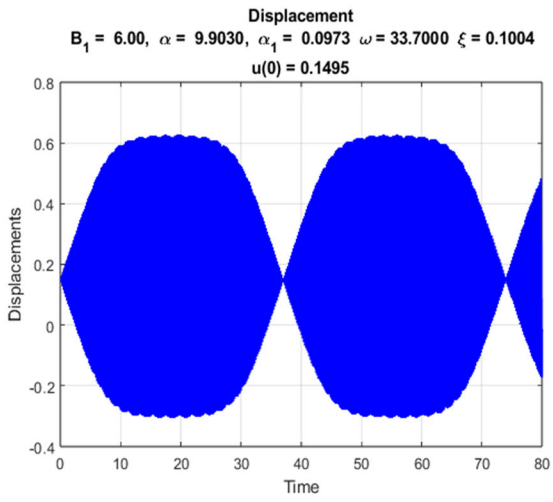

$\alpha_1 < \alpha_{1\,pi}$

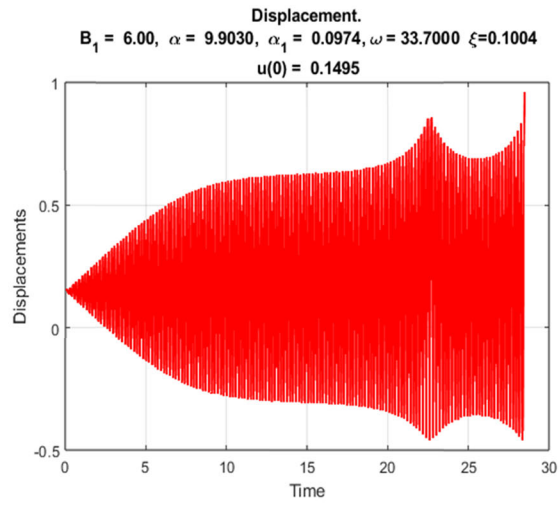

$\alpha_1 > \alpha_{1\,pi}$

Fig. 11 Vibrations (beats) for $\omega \approx \omega_{rf},\ b = 1,\ B_1 = 6.00$

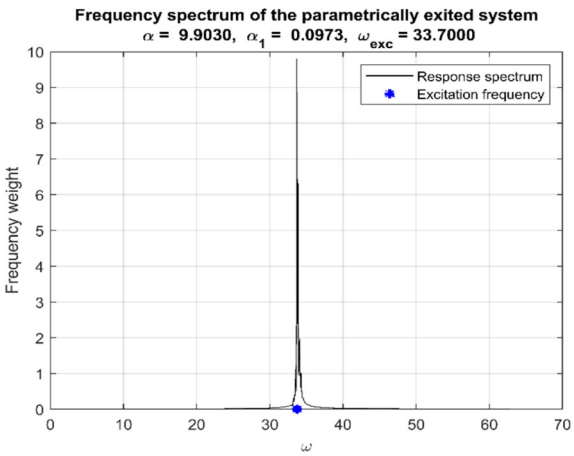

Fig. 12 Frequency spectrum of the parametrically excited system for $\omega \approx \omega_{rf},\ b = 1,\ B_1 = 6.00, \alpha < \alpha_{pi}$

9 The spectral analysis of some characteristic special cases

It is interesting to analyze the vibrations described by Eq. (10) in the presence of parametric excitation, that is, for $\alpha_1 \neq 0$. Equation (10) was integrated numerically. The solutions obtained for a DC value $\alpha = 9.9030$, and for various AC frequencies are presented in Figs. 11, 13, 15. All other parameters are defined in (17).

Figure 11 shows that beats form when the system oscillates at two close frequencies with approximately equal amplitudes. In this case, the parametric excitation frequency is very close to the natural frequency of the system.

Additional information concerning the behaviour of the system can be obtained using a spectral analysis (FFT).

The system response consists of two frequencies: the excitation frequency and the natural frequency. In Fig. 12 (the pure resonance case) these frequencies practically coincide.

Figure 13 shows the solution of Eq. (10) for the same DC and AC amplitudes as in Fig. 11, but for an excitation frequency 4 times less than the natural frequency of the system. The amplitude of the solution at $\omega \approx \omega_{nf}$ is much greater than the amplitude of the solution at $\omega \approx \omega_{nf}/4$.

When excited at a frequency corresponding to a quarter of the resonant frequency, the main response of the system still occurs at the frequency of the primary resonance (see Fig. 14).

If the excitation takes place at a certain intermediate frequency, a multi-frequency mode occurs (see Figs. 15, 16). The frequency spectrum of the solution of Eq. (10) for parametric excitations was studied at excitation frequencies $\frac{6}{24}\omega_{rf}, \frac{7}{24}\omega_{rf}, \frac{8}{24}\omega_{rf}, \frac{5}{12}\omega_{rf}, \frac{1}{2}\omega_{rf}$, $0{:}813X_{nf}, \omega_{rf}, \frac{3}{2}\omega_{rf}, 2\omega_{rf}$. In all cases, the system

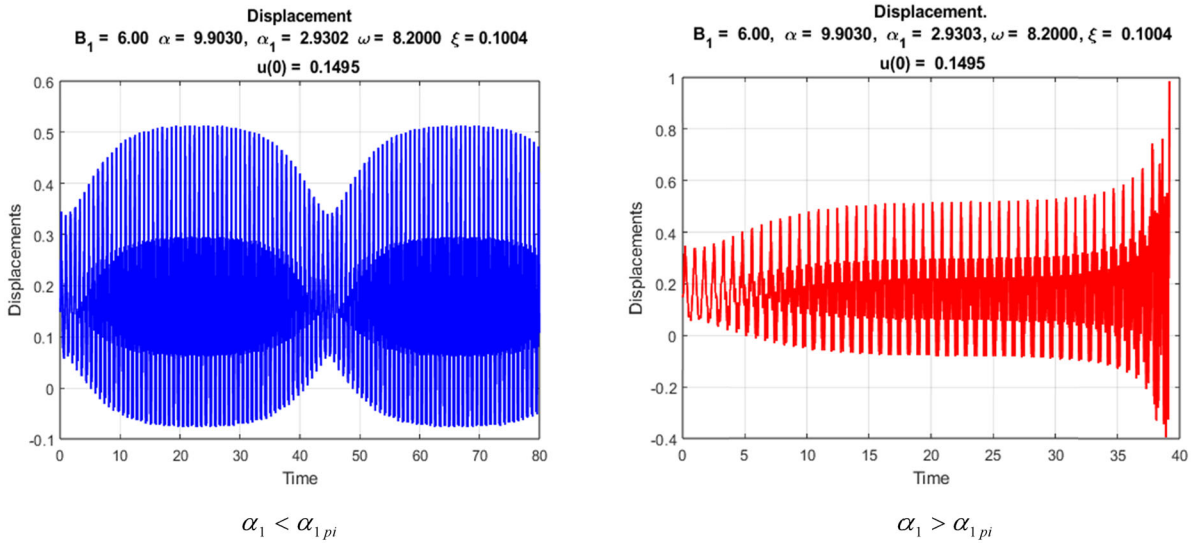

$\alpha_1 < \alpha_{1\,pi}$ $\qquad$ $\alpha_1 > \alpha_{1\,pi}$

Fig. 13 Vibrations (superharmonic resonance) for $\omega \approx \omega_{nf}/4,\ b = 1,\ B_1 = 6.00$

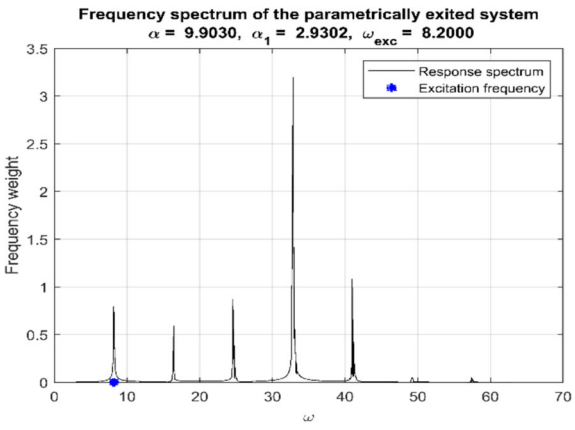

Fig. 14 Frequency spectrum of the parametrically excited system for $\omega \approx \omega_{nf}/4,\ \ b = 1,\ B_1 = 6.00;\ \ \alpha_1 < \alpha_{1\,pi}$

response consists of the excitation frequency, the primary resonance frequency, and possibly additional frequencies. In cases where the primary resonance frequency is a multiple of the excitation frequency, the response at the primary resonance frequency significantly exceeds the response at the excitation frequency (Fig. 14). In other cases, the response at the excitation frequency is greater than the response at the primary resonant frequency (Fig. 16).

10 Analysis of the resonances

The presence of resonances in the original system can play both a negative and a positive role. For example, using resonances, one can significantly reduce the voltage for which the system leads to a pull-in [46]. On the other hand, there may be a problem of reducing or suppressing the emerging resonances. In both cases, it is important to understand that the resonances that arise in the system have different origins. These can be nonlinear resonances due to a forcing, or parametric resonances due to a parametric excitation of the system, or a combination of these resonances. The rate of increase in amplitude of the response of a system with parametric resonance is usually exponential in time, whereas the typical nonlinear resonance is usually characterized by a linear growth rate in time. To reduce or suppress resonances, one can increase damping to absorb vibration energy, or adjust system parameters to move away from resonance frequencies, or one can modify the excitation frequency or amplitude. The efficiency of the indicated approaches depends on the type of resonance. So, information about the origins of the resonances occurring in the system is important from a practical point of view.

The presence of excitations of different origins in the original system can be easily seen by rewriting Eq. (10) for $\alpha = 0$, $I_2 = I_3 = 0$ as follows

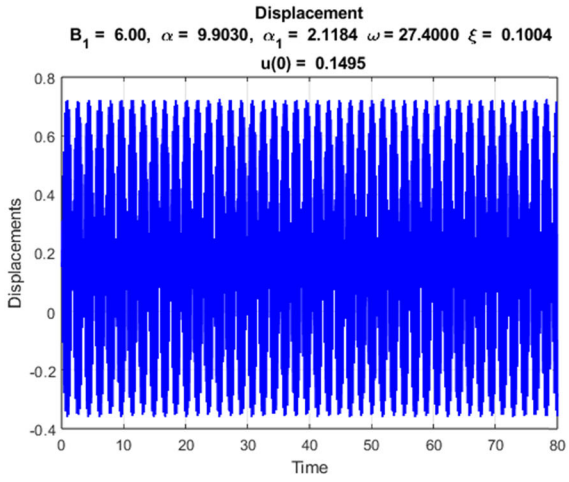

$\alpha_1 < \alpha_{1\,pi}$

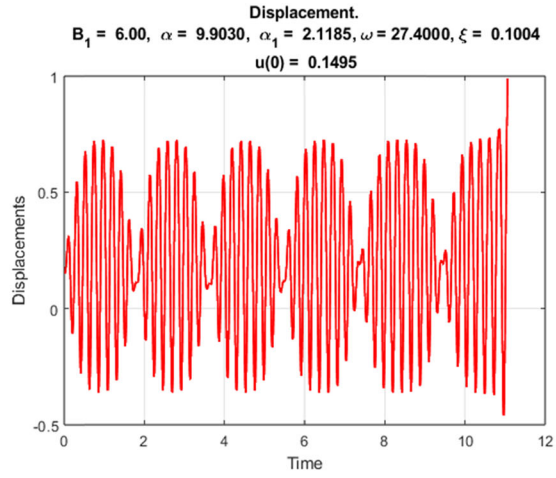

$\alpha_1 > \alpha_{1\,pi}$

Fig. 15 Vibrations for $\omega \approx 0.813\omega_{nf},\ b = 1,\ B_1 = 6.00$

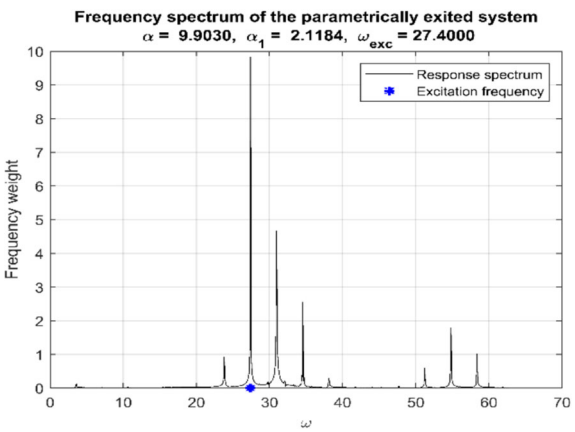

Fig. 16 Frequency spectrum of the parametrically excited system for $\omega \approx 0.813\omega_{nf},\ b = 1,\ B_1 = 6.00;\ \ \alpha_1 < \alpha_{1\,pi}$

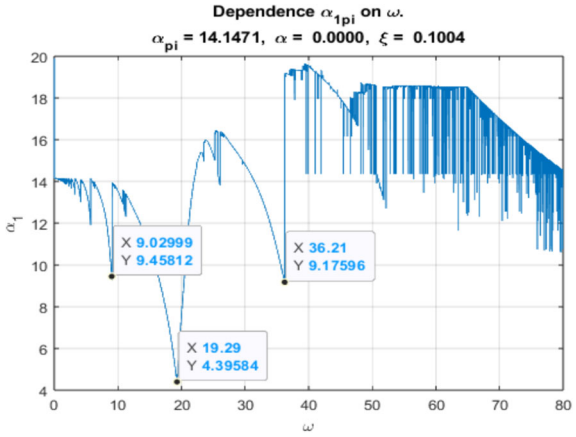

Fig. 17 Dependence of the dimensionless dynamic pull-in $\alpha_{1\mathrm{pi}}$ on the dimensionless frequency ω in the absence of a DC voltage ($\alpha = 0$)

$$\ddot{u} + \xi\dot{u} + c_1 u + c_3 u^3 = \frac{8}{9}\varphi_2\alpha_1^2(\cos 2\omega t - 1) + \frac{32}{9}\varphi_1\alpha_1^2(\cos 2\omega t - 1)\left(I_1(u) - \frac{1}{4}\right) \tag{24}$$

The parameter φ_i takes the value 0 or 1. For $\varphi_1 = \varphi_2 = 1$ one obtains the original system. The term in the Eq. (24) with φ_1 determines a parametric excitation, and the one with φ_2 a force excitation. Note that the frequency of both excitations is equal to twice the frequency of the applied AC.

Figure 17 shows the dependence of the dimensionless dynamic pull-in $\alpha_{1\mathrm{pi}}$ on the dimensionless frequency ω in the absence of DC voltage ($\alpha = 0$). It is easy to see that at points $\omega \approx 9.0,\ \omega \approx 19.3,\ \omega \approx 36.2$ the value of the dynamic pull-in $\alpha_{1\mathrm{pi}}$ is significantly less than at other neighboring points, which can be explained by the presence of resonances at these points.

Let us perform some numerical experiments, by neglecting parametric excitation in one case, that is, assuming that $\varphi_1 = 0, \varphi_2 = 1$, and by discarding force excitation in the other case by setting $\varphi_1 = 1,\ \varphi_2 = 0$. Note that purely-parametric electrostatic actuation is realized in the case of a differential capacitor [48]. The

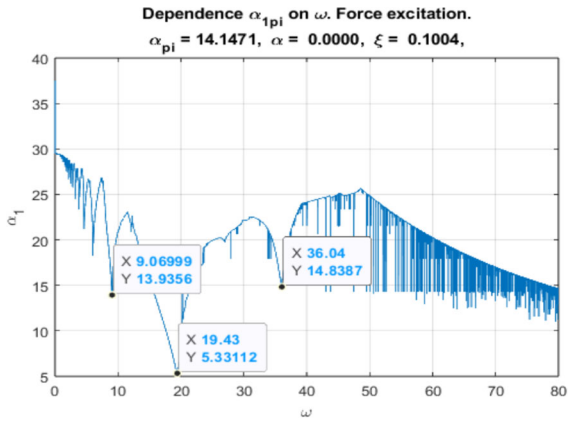

Fig. 18 Dependence of the dimensionless dynamic pull-in α_{1pi} on the dimensionless frequency ω for Eq. (24) with $\varphi_1 = 0$, $\varphi_2 = 1$ (force excitation)

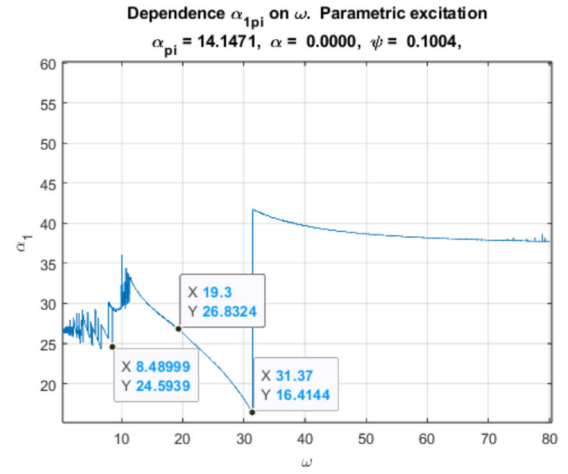

Fig. 19 Dependence of the dimensionless dynamic pull-in α_{1pi} on the dimensionless frequency ω for Eq. (24) with $\varphi_1 = 1$, $\varphi_2 = 0$ (parametric excitation)

numerical results are presented in Figs. 18 and 19. These curves do not describe the behavior of the complete, original system, but allows one to qualitatively trace the influence of the factors of force excitation (Fig. 18) or parametric excitation (Fig. 19).

At the points $\omega \approx 9.1$, $\omega \approx 19.4$, $\omega \approx 36.0$ (Fig. 18) the values of the dynamic pull-in, as well as in Fig. 17, are significantly less than at other neighboring points. This confirms the presence of resonances caused by a driving force. We also note that the chaotic behavior of an electromechanical system at high excitation frequencies qualitatively coincides with the behavior of a force driven Duffing equation [49].

In Fig. 19, in the neighborhood of the point $\omega \approx 19.3$, the dynamic pull-in does not reach an extremum at all. At the points $\omega \approx 8.5$ and $\omega \approx 31.4$, the dynamic pull-in reaches local minimum values $\alpha_{1pi} \approx 24.6$ and $\alpha_{1pi} \approx 16.3$. This allows us to assume the presence of parametric resonances at these points. In addition, judging by the discontinuous behavior of the solutions, these points may be bifurcation points.

The results of the experiments are summarized in Table 3.

Based on the results as presented in Table 3, it can be concluded that for $\omega \approx 9.0$ and $\omega \approx 36.2$ there are resonances caused by both force and parametric excitation, and for $\omega \approx 19.3$ there is a resonance caused by a force excitation.

11 Conclusions

In this paper the behavior of electrically actuated nonlinear clamped rectangular micro- and nanoplates under the action of DC and AC voltages is studied. The geometric nonlinearity of the plate is taken into account within the framework of Berger's hypothesis. Using the Kantorovich method, the original PDE is reduced to an ODE with respect to the time variable. An algorithm has been developed for determining the amplitudes and corresponding frequencies of alternating voltage at which pull-in occurs.

Model and algorithm validations have been obtained by comparing the results obtained in this paper with those obtained in the existing literature. Closeness of these results confirms the adequacy of the adopted model and the high accuracy of the presented algorithm. A study was conducted for a wide range of frequencies and ratios between the amplitudes of the DC and AC voltages. Along with the determination of the pull-in values, the behavior of the displacements over time was studied. A spectral analysis was also conducted, which allowed us to analyze the relationships between excitation frequencies and response spectra.

The calculations were performed for a wide range of AC frequencies, that is, for frequencies from 0 to approximately $2\omega_{rf}$, where ω_{rf} is the primary resonance frequency of the system (Figs. 9 and 10). For

Table 3 Results of the experiments to determine the nature of the emerging resonances

Equation (10),$\varphi_1 = 1,\ \varphi_2 = 1$	$\omega \approx 9.0,\ \alpha_{1pi} \approx\ 9.5$	$\omega \approx 19.3,\ \alpha_{1pi} \approx 4.4$	$\omega \approx 36.2,\ \alpha_{1pi} \approx\ 9.2$
Equation (24),$\varphi_1 = 0, \varphi_2 = 1$	$\omega \approx 9.1,\ \alpha_{1pi} \approx 13.9$	$\omega \approx 19.4,\ \alpha_{1pi} \approx 5.2$	$\omega = 36.0,\ \alpha_{1pi} \approx 14.8$
Equation (24),$\varphi_1 = 1, \varphi_2 = 0$	$\omega \approx 8.5,\ \alpha_{1pi} \approx 24.6$		$\omega \approx 31.4,\ \alpha_{1pi} \approx 16.3$

small values of the dimensionless frequency ω (in the interval from $\omega = 0$ up to approximately $\omega = 4$), the values of the dynamic pull-in differ little from the static pull-in values. Therefore, if the AC frequency does not exceed 10–11% of ω_{rf}, one can focus on static pull-in. Figure 10 shows that the parameter $\alpha + \alpha_1$, characterizing the maximum voltage value for a given frequency, describes the system behavior well. An increase in the AC frequency leads to a dramatic change in the pull-in values. This is caused by different kinds of resonances. These resonances can be nonlinear resonances due to forcing, or can be parametric resonances. To clarify the origins of the emerging resonances, we conducted some numerical experiments, neglecting in one case the terms causing parametric excitation, and in the other case—the terms causing force excitation.

Figure 17 shows that a significant decrease in dynamic pull-in values is observed for frequencies approximately equal to ω_{rf}, $\omega_{rf}/2$, $\omega_{rf}/3$, $\omega_{rf}/4$, $\omega_{rf}/5$ as well as for a number of smaller discrete frequency values. Using the numerical results in Fig. 18, it is easy to verify that for point $\omega = \omega_{rf}/2$ we have a primary nonlinear resonance (since the excitation frequency is equal to twice the AC frequency). For $\omega = \omega_{rf}$ we have a subharmonic resonance, and for $\omega_{rf}/3$, $\omega_{rf}/4$, $\omega_{rf}/5$ superharmonic resonances occur. There are also higher-order superharmonic resonances that do not have a strong effect on a reduction of the AC voltage amplitude. The behavior of the solution for $\omega > \omega_{rf}$ is determined by the force component of the excitation and apparently leads to a sequence of bifurcations.

Figure 19 demonstrates the presence of a principal parametric resonance in the system for a frequency somewhat lower than $\omega = \omega_{rf}$. In the original system, as can be seen from Fig. 17, for $\omega \approx \omega_{rf}$ a nonlinear and a parametric resonance interact, and as a result the pull-in value turns out to be lower than the ones under the influence of the force or parametric excitation alone. The influence of parametric resonances of fractional order is much smaller. After the principal parametric resonance, the system enters the stability region under parametric excitations. Thus, the main factor influencing the decrease of dynamic pull-in for the system under consideration is the primary nonlinear resonance at $\omega = \omega_{rf}/2$. The performed analysis provides useful information in practical situations. Knowing the resonant frequencies allows us to avoid them in operating electromechanical systems. This can be achieved by changing the AC voltage frequency or by modifying the parameters of the system itself. On the other hand, knowledge of the resonant frequencies also allows us to design new and more effective devices that use a voltage much lower than the traditionally used ones [46].

This work can be expanded in several directions. It is interesting to study the possibility to reduce or suppress resonances using nonlinear friction [50] or high-frequency vibration control [51]. Thinking about unaccounted factors, it is of interest to study the effect of applied loads and the influence of boundary conditions. Determining these factors in experiments is difficult. Theoretical research can provide some boundaries for changes in pull-in values and for trends in their change.

For a more accurate description of the capacitance of a rectangular parallel-plate structure, fringing corrections [52] and higher order correction of electrostatic pressure [53] can be taken into account.

The obtained nonlinear problem deserves a more detailed study. First of all, we are talking about investigation of the stability of caused by AC voltage vibrations, because in a number of papers the possibility of chaotic behavior of the system near pull-in values are observed [12, 17].

Acknowledgements Andrianov I.V. thanks TU Delft for hospitality during October 2023.

Author contributions I.V. Andrianov: conceptualization, investigation, writing and original draft preparation, writing, review, and editing; W.T. van Horssen: conceptualization, methodology, investigation, writing, review, and editing; S.G. Koblik: methodology, investigation, software, formal analysis; G.A. Starushenko: methodology, investigation, software, formal

analysis, writing and original draft preparation. All authors have read and agreed to the published version of the manuscript.

Funding This research was partly funded by the Science Committee of the Ministry of Science and Higher Education of the Republic of Kazakhstan (Grant No. AP 23490543) (for Andrianov I.V.) and was partly supported by a grant from the Simons Foundation (Award ID: 1160642, Project Title: Simons Foundation Support to Researchers in Ukraine, Program: Presidential Discretionary-Ukraine Support Grants) (for Starushenko G.A.).

Data availability No datasets were generated or analysed during the current study.

Declarations

Conflict of interest The authors declare no competing interests.

References

1. Younis, M.I.: MEMS: Linear and Nonlinear Statics and Dynamics. Springer, Berlin (2011)
2. Zhang, W.M., Yan, H., Peng, Z.K., Meng, G.: Electrostatic pull-in instability in MEMS/NEMS: a review. Sens. Actuators A: Phys. **214**, 187–218 (2014)
3. Khaniki, H.B., Ghayesh, M.H., Amabili, M.: A review on the statics and dynamics of electrically actuated nano and micro structures. Int. J. Non-Lin. Mech. **129**, 103658 (2021)
4. Khan, F., Younis, M.I.: RF MEMS electrostatically actuated tunable capacitors and their applications: a review. J. Micromech. Microeng.Micromech. Microeng. **32**(1), 013002 (2002)
5. Corigliano, A., Ghisi, A., Mariani, S., Zega, V.: Mechanics of microsystems: recent journey in a fascinating branch of mechanics. In: Rega, G. (ed.) 50+ Years of AIMETA, pp. 419–435. Cham, Springer (2022)
6. Wygant, I.: A comparison of CMUTs and piezoelectric transducer elements for 2D medical imaging based on conventional simulation models. In: 2011 IEEE Intern. Ultrasonics Symp., 100–103 (2011)
7. Kravetc, P., Gendelman, O.: Approximation of potential function in the problem of forced escape. J. Sound Vib.Vib. **526**, 116675 (2022)
8. Rosenau, Ph., Krylov, S.: Solitary waves in electro-mechanical lattices. Chaos **33**, 123124 (2023)
9. Bouchaala, A., Jaber, N., Shekhah, O., Chernikova, V., Eddaoudi, M., Younis, M.I.: A smart microelectromechanical sensor and switch triggered by gas. Appl. Phys. Lett. **109**(1), 013502 (2016)
10. Hajjaj, A.Z., Jaber, N., Ilyas, S., Alfosail, F.K., Younis, M.I.: Linear and nonlinear dynamics of micro and nano-resonators: review of recent advances. Int. J. Non-Lin. Mech. **119**, 103328 (2020)
11. Rhoads, J.F., Shaw, S.W., Turner, K.L.: Nonlinear dynamics and its applications in micro- and nanoresonators. J. Dyn. Sys. Meas. Control. **132**(3), 034001 (2010)
12. Saghir, S., Younis, M.I.: An investigation of the static and dynamic behavior of electrically actuated rectangular microplates. Int. J. Non-Lin. Mech. **85**, 81–93 (2016)
13. Tajalli, S.A., Zand, M.M., Ahmadian, M.T.: Dynamic analysis of electrically actuated rectangular microplates with nonlinear plate theory under squeeze-film damping effect. In: Proc. IMECE2008 ASME Int. Mech. Eng. Cong. Expos. Oct 31–Nov 6, 2008, Boston, Massachusetts, USA (8 pages) (2008)
14. Zhao, X., Abdel-Rahman, E.M., Nayfeh, A.H.: A reduced-order model for electrically actuated microplates. J. Micromech. Microeng.Micromech. Microeng. **14**, 900–906 (2004)
15. Rezazadeh, G., Talebian, S., Fathalilou, M.: Dynamic pull-in phenomenon in the fully clamped electrostatically actuated rectangular microplates considering damping effects. Sens. Transducers J. **103**(4), 122–131 (2009)
16. Zand, M.M., Ahmadian, M.: Vibrational analysis of electrostatically actuated microstructures considering nonlinear effects. Commun. Nonlinear Sci. Numer. Simul.. Nonlinear Sci. Numer. Simul. **14**, 1664–1678 (2009)
17. Benedetti, K.C.B., Goncalves, P.B., Lenci, S., Rega, G.: Parameter uncertainty and noise effects on the global dynamics of an electrically actuated microarch. J. Micromech. Microeng.Micromech. Microeng. **33**, 064001 (2023)
18. Batra, R.C., Porfiri, M., Spinello, D.: Reduced-order models for microelectromechanical rectangular and circular plates incorporating the Casimir force. Int. J. Solids Struct.Struct. **45**(11–12), 3558–3583 (2008)
19. Batra, R.C., Porfiri, M., Spinello, D.: Effect of van der Waals force and thermal stress on pull-in instability of microplates. Sensors **8**(2), 1048–1069 (2008)
20. Chao, P.C., Chiu, C.-W., Tsai, C.: A novel method to predict the pull-in voltage in a closed form for micro-plates actuated by a distributed electrostatic force. J. Micromech. Microengin. **16**, 986–998 (2006)
21. Harjanto, E., van Horssen, W.T., Tuwankotta, J.M.: On resonances in a weakly nonlinear microbeam due to an electric actuation. Nonlin. Dyn. **104**(4), 3157–3185 (2021)
22. Nathanson, H.C., Newell, W.E., Wickstrom, R.A., Davis, J.R.: The resonant gate transistor. IEEE Trans. Electron Devices **14**(3), 117–133 (1967)
23. Llibre, J., Nuñez, D.E., Rivera, A.: Periodic solutions of the Nathanson's and the comb-drive models. Int. J. Non-Lin. Mech. **104**, 109–115 (2018)
24. Alsaleem, F.M., Younis, M.I., Ruzziconi, L.: An experimental and theoretical investigation of dynamic pull-in in MEMS resonators actuated electrostatically. J. Microelectromech. Syst.Microelectromech. Syst. **19**(4), 794–806 (2010)
25. Ruzziconi, L., Ramini, A.H., Younis, M.I., Lenci, S.: Theoretical prediction of experimental jump and pull-in dynamics in a MEMS sensor. Sensors **14**, 17089–17111 (2014)
26. Kalhori, H., Shooshtari, A., Tashakori, S., Li, B.: Mechanical behavior of a rectangular capacitive micro-plate subjected to an electrostatic load. Int. J. Dyn. Contr. **10**, 1337–1348 (2022)

27. Stewart, I.W., Faulkner, T.R.: Estimating the escape zone for a parametrically excited pendulum-type equation. Phys. Rev. E **62**(4), 4856–4861 (2000)
28. Farokhi, H., Ghaesh, M.H.: Nonlinear mechanics of electrically actuated microplates. Int. J. Eng. Sci. **123**, 197–213 (2018)
29. Karimzade, A., Moeenfard, H., Ahmadian, M.T.: Nonlinear analysis of pull-in voltage for a fully clamped microplate with movable base. In: Proc. ASME 2012 Int. Mech. Engin. Congress and Exposition, ASME, pp. 71–75 (2012)
30. Rosi, G., Pouget, J., dell'Isola, F.: Control of sound radiation and transmission by a piezoelectric plate with an optimized resistive electrode. Eur. J. Mech. A/Solids **29**, 859–870 (2010)
31. Andrianov, I.V., Awrejcewicz, J., Koblik, S.G., Starushenko, G.A.: Nonlinear oscillation of a microbeam due to an electric actuation – comparison of approximate models. ZAMM **104**(2), e202300091 (2024)
32. Andrianov, I.V., Koblik, S.G., Starushenko, G.A.: Investigation of electrically actuated geometrically nonlinear clamped circular nanoplate. Acta Mech. Mech. **235**(2), 1015–1026 (2024)
33. Bordag, M.: Casimir effect for a sphere and a cylinder in front of a plane and corrections to the proximity force theorem. Phys. Rev. D **73**, 125018 (2006)
34. Klimchitskaya, G.L., Mohideen, U., Mostepanenko, V.M.: Casimir and van der Waals forces between two plates or a sphere (lens) above a plate made of real metals. Phys. Rev. A **61**, 062107 (2000)
35. Israelachvili, J.N.: Intermolecular and Surface Forces, 2nd edn. Academic Press, London (1991)
36. Berger, H.M.: A new approach to analysis of large deflections of plates. Trans. ASME J. Appl. Mech. **22**(4), 465–472 (1955)
37. Krommer, M., Irschik, H.: Post-buckling of piezoelectric thin plates. Int. J. Struct. Stab. Dyn.Struct. Stab. Dyn. **15**(7), 1540020 (2015)
38. Svačina, R., Machalová, J.: Analysis of Berger nonlinear elastic static plate bending of rectangular plates. Math. Mech. Solids **28**(11), 2458–2490 (2023)
39. Peradze, J.: A Kirchhoff type equation in a nonlinear model of shell vibration. ZAMM **97**(2), 144–158 (2017)
40. Dickinson, S.M., Li, E.K.H.: On the use of simply supported plate functions in the Rayleigh-Ritz method applied to the flexural vibration of rectangular plates. J. Sound Vib.Vib. **80**(2), 292–297 (1982)
41. Kantorovich, L.V., Krylov, V.I.: Approximate Methods of Higher Analysis. Noordhoff, Groningen (1958)
42. Abramowitz, M., Stegun, I.A. (eds.): Handbook of Mathematical Functions, with Formulas, Graphs, and Mathematical Tables. Dover, New York (1965)
43. Elsgolts, L.: Differential Equations and the Calculus of Variations. Mir, Moscow (1977)
44. Ananthasuresh, G.K., Gupta, R.K. Senturia, S.D.: An approach to macromodeling of MEMS for nonlinear dynamic simulation. In: Proceedings of the ASME International Conference of Mechanical Engineering Congress and Exposition (MEMS). Atlanta, GA, pp. 401–407 (1996)
45. Krylov, S., Maimon, R.: Pull-in dynamics of an elastic beam actuated by distributed electrostatic force. In: Proceedings of the 19th Biennial Conference in Mechanical Vibration and Noise (VIB), Chicago, IL, Paper DETC2003/VIB-48518 (2003)
46. Nayfeh, A.H., Younis, M.I., Abdel-Rahman, E.M.: Dynamic pull-in phenomenon in MEMS resonators. Nonlinear Dyn.Dyn. **48**, 153–163 (2007)
47. Najar, F., Nayfeh, A.H., Abdel-Rahman, E.M., Chora, S., Elborgi, S.: Nonlinear analysis of MEMS electrostatic microactuators: primary and secondary resonances of the first mode. J. Vib. ControlVib. Control **16**(9), 1321–1349 (2010)
48. Rhoads, J.F., Shaw, S.W., Turner, K.L.: The nonlinear response of resonant microbeam systems with purely-parametric electrostatic actuation. J. Micromech. Microeng.Micromech. Microeng. **16**, 890–899 (2006)
49. Szemplinska-Stupnicka, W., Niezgodzki, P.: The approximate approach to chaos phenomena in oscillators having single equilibrium position. J. Sound Vib.Vib. **141**(2), 181–192 (1990)
50. Farokhi, H., Rocha, R.T., Hajjaj, A.Z., Younis, M.I.: Nonlinear damping in micromachined bridge resonators. Nonlinear Dyn.Dyn. **111**, 2311–2325 (2023)
51. Sahoo, P.K., Chatterjee, S.: High-frequency vibrational control of principal parametric resonance of a nonlinear cantilever beam: theory and experiment. J. Sound Vib.Vib. **505**, 116138 (2021)
52. Hosseini, M., Zhu, G., Peter, Y.-A.: A new formulation of fringing capacitance and its application to the control of parallel-plate electrostatic micro actuators. Analog Integr. Circ. Sig. ProcessIntegr. Circ. Sig. Process **53**, 119–128 (2007)
53. Krylov, S., Seretensky, S.: Higher order correction of electrostatic pressure and its influence on the pull-in behavior of microstructures. J. Micromech. Microeng.Micromech. Microeng. **16**, 1382–1396 (2006)